# Mean field theory of spherical gravitating systems

Peter J. Klinko and Bruce N. Miller
*Department of Physics, Texas Christian University, Fort Worth, Texas 76129*
(Received 1 March 2000)

Important gaps remain in our understanding of the thermodynamics and statistical physics of self-gravitating systems. Using mean field theory, here we investigate the equilibrium properties of several spherically symmetric model systems confined in a finite domain consisting of either point masses or rotating mass shells of different dimension. We establish a direct connection between the spherically symmetric equilibrium states of a self-gravitating point mass system and a shell model of dimension 3. We construct the equilibrium density functions by maximizing the entropy subject to the usual constraints of normalization and energy, but we also take into account the constraint on the sum of the squares of the individual angular momenta, which is also an integral of motion for these symmetric systems. Two statistical ensembles are introduced that incorporate the additional constraint. They are used to investigate the possible occurrence of a phase transition as the defining parameters for each ensemble are altered.

PACS number(s): 45.05.+x, 05.45.−a

## I. INTRODUCTION

The observation that a number of different types of astronomical objects appear to be in thermodynamically relaxed states has motivated theorists to understand the thermodynamics and statistical physics of self-gravitating systems. Of particular note are the globular clusters, consisting of about a million stars. Besides having relaxed cores, these structures appear to be organized in two distinct classes characterized by radically different density profiles, x-ray production, and other features [1]. This suggests that globular clusters may exist in different thermodynamic phases. However, in contrast with normal ''chemical'' systems, which have been successfully described by thermodynamics at the macroscopic level, both the infinite range and short distance singularity of the Newtonian gravitational potential introduce problems in the statistical theory of phase transitions which make their analysis a challenging task. The description of the system can be simplified by going to the Vlasov limit, i.e., by letting the number of particles become large while controlling the total mass $M$ and energy $E$. In this limit the system is described by the single-particle density $f(x,v,t)$ in the $\mu$ (position, velocity) space, which is employed by most of the standard treatments, including the present work [2]. We refer to this reduced description as mean field theory (MFT). While MFT avoids the problem of dealing with an $N$-body formulation, the difficulties introduced by the singularity and long range of the potential persist.

In the early 1960s Antonov investigated the equilibrium behavior of isolated gravitational systems in MFT [3]. To circumvent the problem of escape, he confined the mass to a finite region by introducing a rigid wall. By fixing the total mass and energy, he showed that maximum entropy solutions for $f$ are spherically symmetric in position and have the expected Maxwellian velocity dependence. However, he proved that there is no *global* maximum to the entropy: while extremal solutions can exist, these are at best *local* maxima. Antonov [3], as well as Lynden-Bell and Wood [4], closely investigated the spherically symmetric system confined in a sphere and showed that when the mass and energy are fixed there are no entropy extrema above a critical radius ($R \gtrsim -0.335GM^2/E$). When the radius is less than this value, the stability of the extremal solutions was studied by several authors (Katz and Lynden-Bell [5], Katz [6,7], Padmanabhan [8,9], and Bavaud [10]). They found that, in general, above a critical density contrast [$\rho(0)/\rho(R) \gtrsim 709$] all extrema are unstable, i.e., they are not *local* maxima. Lynden-Bell and Wood termed this phenomenon the *gravothermal catastrophe* and it is also referred to as the Antonov instability. In such a system, there is no upper bound on the entropy and a state of arbitrarily large entropy can be constructed from a centrally concentrated density profile by shifting more of the mass toward the center (core-halo structures have higher entropy).

More recently, Kiessling [11] has investigated the thermodynamic stability of the full $N$-body point mass system confined in a spherical box using the canonical ensemble. To avoid the short range singularity, he regularized the Newtonian interaction by softening it (letting the potential approach a finite value as the origin is closely approached). He showed that in the limit that the softening vanishes (Newtonian interaction), the canonical equilibrium measure is the superposition of Dirac measures at any temperature, meaning that the system is in a collapsed point mass state. We have to emphasize that this is the equilibrium solution when the system is in thermal equilibrium with a heat bath. Also, based on the results for the finite $N$-particle system, with proper scaling of the particle mass as we take the mean field limit, he showed that the single-particle density function is proportional to the Dirac distribution. Therefore the system's equilibrium state is the collapsed state in the canonical ensemble. Kiessling's conclusions do not contradict the earlier work applying MFT to the microcanonical ensemble (fixed mass and energy) described above, since no global entropy maximum was found in that case either.

In fact, the pure Newtonian potential is never a correct picture in general because of the finite size of stars and atoms. In a nearly hidden Appendix of their paper describing the gravothermal catastrophe, it was first pointed out by Lynden-Bell and Wood that if we modify the singular $1/r$

 

Newtonian gravitational potential at the center by introducing a small minimal distance between the particles (the so-called hard-sphere model) complete collapse will be avoided and a global entropy maximum should exist [4]. They further conjectured that in this situation a first order phase transition to a centrally concentrated core-halo configuration would occur as the system energy is reduced. Several authors demonstrated the existence of a phase transition in special mean field models with a modified gravitational potential. Hertel and Thirring [12] were the first to show analytically that a gravitating system can undergo a first-order phase transition. Although their system is not purely gravitational and has no singularity, the pair-interaction potential is purely attractive and has a fixed value when the pair of particles are in a given subdomain. Also, Lynden-Bell and Lynden-Bell [13] showed the occurrence of a first-order phase transition in their special gravitational system, consisting of point particles distributed on a shell that cannot shrink into a point mass (inner boundary) or expand to infinity (outer boundary). Kiessling *et al.* also applied the hard-sphere model [14] to study planet formation: They were able to explain the existence of observable planets by showing that the mass belonging to the condensed phase is well below the Jeans mass [2]. For finite $N$-body systems, a gravitational first-order phase transition was first observed dynamically by Miller and Youngkins [15]. They investigated a model consisting of irrotational, concentric, spherical mass shells confined between two rigid spherical boundaries. The system was studied both theoretically in the mean field limit and numerically by $N$-body simulations in the microcanonical, canonical, and grand canonical ensembles. The analysis for this one-dimensional system showed that the system undergoes a first-order phase transition instead of a gravothermal catastrophe. As expected in gravitational systems, there were some discrepancies in the results for different ensembles; however, the numerical $N$-shell simulations were always in good agreement with the corresponding mean field predictions.

Much earlier, Eddington [16] determined the form of the general stationary solution of the Vlasov equation for a spherical system with an anisotropic velocity distribution that obeys the Schwarzschild law [2]. This model explicitly depends on the square of the angular momentum $l^2$, but it also includes the isothermal part: $f(\mathbf{r},\mathbf{v}) \propto e^{-\beta\epsilon} e^{-\gamma l^2}$. The model was presented in 1915, but it may have been forgotten. Later, several phenomenological models were improved by including Eddington's anisotropic term (King-Michie models and others [17,1,2]), giving a better fit to the observed density profiles of globular clusters. However, in some cases, a good fit was not obtained for globular clusters with core-halo structures. In other words, a fair number of globular clusters that have a small and very dense core surrounded by a thin halo structure do not obey these empirical density-fit models. On the other hand, in addition to the system energy, the sum of the angular momentum squares $L_2 = \Sigma l_i^2$ is also an integral of the motion for any isolated spherically symmetric system in the mean field limit [2], and should not be ignored.

The purpose of our work is to present a more general approach for investigating the equilibrium properties of confined, spherical systems than those mentioned above, which takes into account both integrals of a spherical gravitating system, and to introduce idealized dynamical ''shell'' models that also satisfy these constraints. Model gravitating systems consisting of a collection of concentric, infinitesimally thin spherical shells were first introduced by Henon [18]. They are useful for investigating the initial stages of evolution of a spherically symmetric self-gravitating system, before the onset of binary formation arising from three-body effects [1]. They have the further advantages of ease and accuracy of algorithm construction, since it is possible to analytically solve for the motion of each shell between encounters, eliminating the need for the tedious and slow stepwise integration of coupled, nonlinear, differential equations [19,15,20].

In the present work we consider the mean field theory of a system of gravitating point particles moving in three-dimensional space, as well as that of thin, rotating, spherical mass shells with angular momentum vectors restricted to manifolds of one, two, and three dimensions. We first determine conditions for the equilibrium one-particle probability density function $f(x,p)$ of a unit mass particle (shell) by finding the entropy extrema with respect to the constraints of (1) the normalization, (2) the system energy $E$, and (3) the sum of the squares of the angular momentum $L_2$. We then show that the introduction of the integral $L_2$ suggests a different type of canonical ensemble $(T\text{-}\gamma)$, in addition to the extension of the microcanonical ensemble $(E\text{-}L_2)$. A nonlinear differential equation governing the radial density valid for each ensemble is derived for the case of the three-dimensional point mass system, and for each shell system. We then prove that the radial density of the shell system with angular momentum confined to the Euclidean plane satisfies the identical differential equation as the three-dimensional point mass system, and we carefully study the equilibrium solutions for this case numerically. The stability of the extremum solutions of each model is investigated in both microcanonical $(E\text{-}L_2)$ and canonical $(T\text{-}\gamma)$ ensembles. At first glance it is natural to anticipate that the centrifugal barrier associated with the additional constraint will eliminate any tendency for complete core collapse without introducing an inner boundary in the system or changing the gravitational potential by other means. We conclude by investigating the possible presence of a phase transition that would remove the gravothermal catastrophe.

## II. THE ENTROPY EXTREMA

### A. Spherically symmetric point mass systems

The primary goal is to evaluate the equilibrium single-particle probability density function $f(x,p)$ that maximizes the entropy in the mean field limit. Consider the spherically symmetric isolated point mass system in three space dimensions with total mass $M$ confined in a sphere of radius $b$. We choose units where $G=M=b=1$ and introduce spherical coordinates $x=(r,\varphi,\vartheta)$. The Lagrangian per unit mass of a single particle moving in the mean field potential $\Phi(r)$ is

$$L=\frac{1}{2}\dot{r}^2+\frac{1}{2}r^2(\dot{\vartheta}^2+\dot{\varphi}^2\sin^2\vartheta)-\Phi(r), \tag{1}$$

where, for a Newtonian pairwise interaction, $\Phi(r)$ is given by

$$\Phi(r) = -\int\int [G(r,r') + G(r',r)] f(x',p') d^3x' d^3p'. \tag{2}$$

Here

$$G(r,r') = \frac{\Theta(r-r')}{r}$$

and, as usual, $\Theta(r)$ denotes the Heaviside step function. The Hamiltonian is then

$$H = \frac{1}{2}v^2 + \frac{l_\vartheta^2}{2r^2} + \frac{l_\varphi^2}{2r^2\sin^2\vartheta} + \Phi(r), \tag{3}$$

where $p = (v, l_\varphi, l_\vartheta)$ are the corresponding canonical momenta. Our plan is first to determine the entropy extrema, and then verify whether or not the solutions are local maxima. The entropy of the system is [2,8]

$$S = -\int\int f \ln f d^3x d^3p, \tag{4}$$

and the constraints for which we need to find the extremum are (1) normalization of $f$, (2) energy conservation in the complete system, and (3) conservation of $L_2$:

$$1 = \int\int f d^3x d^3p, \tag{5}$$

$$L_2 = \int\int l^2 f d^3x d^3p, \tag{6}$$

$$E = \int\int f\left(\frac{1}{2}v^2 + \frac{1}{2r^2}l^2 + \frac{1}{2}\Phi(r)\right) d^3x d^3p, \tag{7}$$

where

$$l^2 = \left(l_\vartheta^2 + \frac{l_\varphi^2}{\sin^2\vartheta}\right).$$

Introducing Lagrange multipliers $\alpha$, $\beta$, $\gamma$ we have an extremum for the functional $S$ when

$$0 = \delta(S - \alpha - \beta E - \gamma L_2). \tag{8}$$

Taking the first variation of each term in Eq. (8), and asserting Eqs. (5), (7), (6), and (2), we obtain

$$0 = -\int\int \left[(\ln f + 1) + \alpha + \beta\left(\frac{1}{2}v^2 + \frac{1}{2r^2}l^2 + \Phi(r)\right) + \gamma l^2\right] \times \delta f d^3x d^3p,$$

from which finally

$$0 = -(\ln f + 1) - \alpha - \beta\left(\frac{1}{2}v^2 + \Phi(r)\right) - \left(\frac{\beta}{2r^2} + \gamma\right) l^2. \tag{9}$$

Thus the one-particle probability density function (PDF) is

$$f = \exp\left[-(\alpha+1) - \beta\left(\frac{1}{2}v^2 + \Phi\right) - \left(\frac{\beta}{2r^2} + \gamma\right) l^2\right]. \tag{10}$$

In order to obtain the radial density $\rho(r)$, we have to integrate $f$ over the other variables. To ensure that the integrals over $v$, $l_\vartheta$, and $l_\varphi$ converge, the following conditions are necessary: $\beta > 0$ and $\beta/2r^2 + \gamma > 0$ at any $r$. Therefore the second condition is $2\gamma/\beta > -1/b^2 = -1$. Using $K = \exp[-(\alpha+1)]$, we get

$$\begin{aligned}\rho(r) &= \int\int f d^3p d\varphi d\vartheta \\ &= \int_0^{2\pi}\int_0^{\pi} K\sqrt{\frac{2\pi}{\beta}}\frac{\pi\sin\vartheta}{\beta/2r^2+\gamma}\exp(-\beta\Phi) d\varphi d\vartheta \\ &= \frac{K(2\pi)^{5/2}}{\sqrt{\beta}}\left(\frac{\beta}{2r^2} + \gamma\right)^{-1} e^{-\beta\Phi(r)}.\end{aligned} \tag{11}$$

The Poisson equation for the gravitational potential in a spherical coordinate system,

$$\Delta\Phi = \frac{1}{r^2}\frac{d}{dr}\left(r^2\frac{d\Phi}{dr}\right) = 4\pi\rho_V,$$

where $\rho_V$ is the volumetric mass density. In some cases, it is more convenient to use the linear (radial) density instead of the volume density:

$$\frac{d}{dr}\left(r^2\frac{d\Phi}{dr}\right) = \rho(r). \tag{12}$$

Note that because $M = 1$ the radial probability density function and the linear mass density function are the same. Introducing a new function $\Psi = \beta\Phi$ and employing Eq. (11) we can rewrite Eq. (12) as

$$\frac{d}{dr}\left(r^2\frac{d\Psi}{dr}\right) = \rho(r) = K(2\pi)^{5/2}\sqrt{\beta}\left(\frac{\beta}{2r^2} + \gamma\right)^{-1} e^{-\Psi(r)},$$

obtaining a closed equation for $\Psi$. This in turn can be simplified by introducing constants $C$ and $\Gamma$,

$$\frac{d}{dr}\left(r^2\frac{d\Psi}{dr}\right) = C\left(\frac{1}{r^2} + \Gamma\right)^{-1} e^{-\Psi(r)}, \tag{13}$$

$$C = K(2\pi)^{5/2}\frac{2}{\sqrt{\beta}} > 0, \tag{14}$$

$$\Gamma = \frac{2\gamma}{\beta} > -1.$$

This is the final form of the differential equation for the scaled potential, which we will solve using numerical methods. Finally, we can evaluate $E$, $L_2$, and $S$ in terms of the Lagrange multipliers, the density $\rho(r)$, and the potential $\Phi(r)$. After integrating Eqs. (7), (6), and (4), we obtain

$$S=\alpha+\frac{5}{2}+\beta\int_0^b \rho\Phi dr, \tag{15}$$

$$L_2=\int_0^b \rho\left(\frac{\beta}{2r^2}+\gamma\right)^{-1} dr, \tag{16}$$

$$E=\frac{1}{2\beta}+\int_0^b \rho\left(\frac{1}{\beta+2\gamma r^2}+\frac{\Phi}{2}\right) dr. \tag{17}$$

### B. Shell systems

In this section we consider the system of spherically symmetric, infinitesimally thin, mass shells confined in a sphere with radius $b$. We can define three basic types of the model with dimensions $d=2,3,4$. The one-dimensional ($d=1$) nonrotating shell system is discussed in [15]. In the $d=2$ case, every shell rotates about a fixed axis. When $d=3$, the rotational axis of every shell is in a fixed plane, while $d=4$ means that every shell can rotate about any arbitrary axis. Therefore we use $d-1$ angles as coordinates. Let us consider these systems in the mean field limit again using units where $M=G=b=1$. With the potential discussed above [Eq. (2)], the Lagrangian and the Hamiltonian of a unit mass shell in a spherical coordinate system are, respectively,

$$L=\frac{1}{2}\dot{r}^2+\frac{1}{3}r^2\sum_{k=1}^{n}\dot{\varphi}_k^2-\Phi(r), \tag{18}$$

$$H=\frac{1}{2}v^2+\frac{3}{4}\frac{\sum_{k=1}^{n} l_k^2}{r^2}+\Phi(r), \tag{19}$$

where $\varphi_k (k=1,2,3)$ are the angles around $x$, $y$, and $z$, the $l_k$ are the $x,y,z$ components of the angular momentum per unit mass, and we have used the fact that the moment of inertia of a shell with unit mass is $(2/3)r^2$. In the equations above, we use $n=d-1$, which is the number of degrees of freedom coming only from rotation. This is a generalization of the previous model, and so is the method to find the equilibrium PDF $f(x,p)$. As in the previous section, in order to get the equilibrium solutions first we have to find the extremum of the entropy:

$$S=-\int\int f\ln f d^{n+1}x d^{n+1}p \tag{20}$$

with respect to the three constraints of normalization, $E$, and $L_2$:

$$1=\int\int f d^{n+1}x d^{n+1}p,$$

$$L_2=\int\int f\left(\sum_{k=1}^{n} l_k^2\right) d^{n+1}x d^{n+1}p, \tag{21}$$

$$E=\int\int f\left(\frac{1}{2}v^2+\frac{3}{4}\frac{\sum_{k=1}^{n} l_k^2}{r^2}+\frac{1}{2}\Phi(r)\right) d^{n+1}x d^{n+1}p. \tag{22}$$

The solution for the variational problem can be obtained easily, and the one-particle density function is now

$$f=\exp[-(\alpha+1)]\exp\left[-\beta\left(\frac{1}{2}v^2+\Phi\right)\right]\times\exp\left[-\left(\frac{3\beta}{4r^2}+\gamma\right)\sum_{k=1}^{n} l_k^2\right]. \tag{23}$$

Therefore the radial mass density function is

$$\rho(r)=\int\int f d^{n+1}p d^n\varphi = K(2\pi)^{(2n+1)/2}\frac{\pi^{n/2}}{\sqrt{\beta}}\left(\frac{3\beta}{4r^2}+\gamma\right)^{-n/2}\exp(-\beta\Phi). \tag{24}$$

From the Poisson equation, again using $\Psi=\beta\Phi$, we find

$$\frac{d}{dr}\left(r^2\frac{d\Psi}{dr}\right)=K(2\pi)^{(2n+1)/2}\pi^{n/2}\sqrt{\beta}\times\left(\frac{3\beta}{4r^2}+\gamma\right)^{-n/2}\exp(-\Psi), \tag{25}$$

which can be simplified to

$$\frac{d}{dr}\left(r^2\frac{d\Psi}{dr}\right)=C\left(\frac{1}{r^2}+\Gamma\right)^{-n/2}e^{-\Psi(r)}, \tag{26}$$

$$C=\frac{2^{(4n+1)/2}}{(3\beta)^{n/2}}\pi^{(3n+1)/2}K\sqrt{\beta}>0, \tag{27}$$

$$\Gamma=\frac{4\gamma}{3\beta}>-1. \tag{28}$$

Comparing the results (26) for the three-dimensional shell system ($n=2$) to that of a three-dimensional point mass system (13), we can see that these two systems are equivalent in so far as Eqs. (13) and (26) have the same form.

It is useful to evaluate $S,L_2$, and $E$ in terms of the Lagrange multipliers, $\rho(r)$, and $\Phi(r)$. The integration of Eqs. (20), (21), and (22) yields

$$S=\alpha+\frac{n+3}{2}+\beta\int_0^b \rho\Phi dr, \tag{29}$$

$$L_2=\frac{n}{2}\int_0^b \rho\left(\frac{3\beta}{4r^2}+\gamma\right)^{-1} dr, \tag{30}$$

$$E=\frac{1}{2\beta}+\int_0^b \rho\left(\frac{3n}{8}\frac{1}{(3/4)\,\beta+\gamma r^2}+\frac{\Phi}{2}\right)dr. \qquad (31)$$

### III. $T$-$\gamma$ ENSEMBLE

In the previous sections we derived expressions for the entropy extremum solutions for our model systems in terms of the local radial density. A third Lagrange multiplier $\gamma$ was introduced to satisfy the extra constraint on $L_2$. Thus specifying $E$ and $L_2$ (and, of course, $M$) defines the analog to the microcanonical ensemble for these systems. Alternatively, by fixing $\beta$ and $\gamma$, we can define the analog of the canonical ensemble, in which $E$ and $L_2$ are not fixed, but their average is determined by $\beta$ and $\gamma$, where $\gamma=\partial S/\partial L_2$. We call this the $T$-$\gamma$ ensemble. It can be modeled by imagining that the system is in contact with a heat bath with constant $\beta$ and also an $l^2$ bath at constant $\gamma$. The $l^2$ bath corresponds to the fact that we allow some $l^2$ exchange between the system and the bath. Since the system is spherically symmetric in position, while the system can also exchange angular momentum with the bath, its vector average will vanish. As an example, we can imagine a globular cluster that is embedded in some large spherically symmetric stellar neighborhood with an isotropic velocity distribution. The mean angular momentum of both system and bath is zero, and only $l^2$ and energy exchange can occur (for the moment, we do not take into account the possibility that particles can escape from the cluster).

In performing calculations it is more convenient to use the $T$-$\gamma$ ensemble than the $E$-$L_2$ microcanonical ensemble because in the latter we have to find the Lagrange multipliers from the given $E$ and $L_2$. As can be seen from Eqs. (15), (16), and (17) this is a nontrivial and laborious task. In this ensemble the relevant thermodynamic potential is an extension of the Helmholz free energy,

$$F=E-\frac{1}{\beta}S+\frac{\gamma}{\beta}L_2, \qquad (32)$$

and equilibrium states, if they exist, minimize $F$.

### IV. STABILITY

From the variational problem, we only know the extremum solutions. In order to separate the unstable solutions from the locally stable, we use the modified method of Poincaré's linear series of equilibria. Following Katz [6,7] we can generalize the method to the case of a functional. From now on, we discuss the generalized version of the method which has to be applied to our models to determine whether an extremum solution is stable or unstable. We outline the method below. Let us assume that we want to find the maximum of the functional $F^*(f,s)$ which depends parametrically on $s$. The function $f:\Omega\to R$, where $\Omega$ is a compact domain $\Omega\in R^3$, and the local maximum of the functional is the stable solution. Suppose we partition $\Omega$ and consider the vector $x\in R^n$ with elements $x_i=f(y_i)$ ($y_i\in\Omega$ is not a coordinate but an indexed element in $\Omega$). Instead of dealing with the functional $F^*$, we can construct a function $F:R^n\to R$ such that $F(x,s)\approx F^*(f,s)$. The accuracy can be controlled by refining the partition (increasing $n$). The problem is then shifted to finding the extrema of $F$:

$$\partial_i F(x,s)=0. \qquad (33)$$

Denote the extremum solutions of the problem by $x=\{X_a(s)\}$ where $a,b=1,\ldots,N$ labels different extremal solutions. Assume that the first and second derivatives of $F$ are continuous in $x$ and $s$, and $\dot{X}_a$ is continuous as well. Assume also that the matrix $(-\partial_i\partial_j F)_a$ has a nondegenerate eigenvalue spectrum, which we may consider to be ordered: $k_{1a}(s)<k_{2a}(s)<\cdots<k_{na}(s)<\cdots$, and further that $(-\partial_i\partial_j F)_a$ is diagonal. (We can always transform it into that form.) Let us evaluate $F$ at the extremum points $x=X_a(s)$ where

$$\partial_i F(X_a,s)=0. \qquad (34)$$

Then, as the parameter $s$ is varied, on the extremum labeled $a$,

$$\begin{aligned}0&=\frac{d}{ds}\partial_i F(X_a,s)\\&=(\partial_s\partial_i F)_a+\sum_{j=1}^{\infty}(\partial_j\partial_i F)_a\dot{X}_a^j\\&=(\partial_s\partial_i F)_a-k_{ia}(s)\dot{X}_a^i, \qquad (35)\end{aligned}$$

$$\dot{X}_a^i=\frac{(\partial_s\partial_i F)_a}{k_{ia}(s)}. \qquad (36)$$

The stability of the extremum is determined by the second derivative of $F_a(s)=F(X_a,s)$,

$$\ddot{F}_a=(\partial_s^2 F)_a+\sum_{i=1}^{n}(\partial_i\partial_s F)_a\dot{X}_a^i=(\partial_s^2 F)_a+\sum_{i=1}^{\infty}\frac{(\partial_s\partial_i F)_a^2}{k_{ia}}. \qquad (37)$$

The stability will change only when one of the $k_{ia}$ changes sign, and a change in stability occurs only at bifurcation or limit points [6,7]. Therefore we have to investigate the dependence of $\ddot{F}_a$ on $s$ in order to decide how the stability changes at an $a$-$b$ bifurcation or limit point. If we look at Eq. (37), we can see that, when a particular $k_{ia}(s)$ changes sign from positive to negative, at that point $\lim_{s\to s_0}\ddot{F}_a=+\infty$ and similarly, from the other $b$ branch, $\lim_{s\to s_0}\ddot{F}_b=-\infty$.

Going back to our original problem, we have to apply the method to our model systems in both the $E$-$L_2$ and $T$-$\gamma$ ensembles. The only difficulty is that the method discussed above allows us to include only systems with one control parameter $s$. In our case, we are free to fix either $E$ or $L_2$ in the $E$-$L_2$ ensemble and $\beta$ or $\gamma$ in the $T$-$\gamma$ ensemble and regard the other as the control parameter. Afterwards, we can change the previously fixed parameter and apply the method again for a wide range of parameter sets. In the $E$-$L_2$ ensemble a natural choice of parameter is $E$ with one fixed

value of $L_2$, as the entropy has to be a local maximum if the system is in a locally stable state. If we are at the extremum solution points,

$$\dot{S} = \frac{dS}{dE} = \frac{\partial S}{\partial E} = \beta. \tag{38}$$

For a different value of $L_2$, we can clearly see which branch of the extremum solutions is unstable. To obtain a complete description we can use the same method if $E$ is fixed:

$$\dot{S} = \frac{dS}{dL_2} = \frac{\partial S}{\partial L_2} = \gamma. \tag{39}$$

In the $T$-$\gamma$ ensemble, first consider the case where we fix $\gamma$, and we are looking for the maximum of the functional $-\beta F$. On a branch of the extremum solutions,

$$\frac{dF}{d\beta} = \frac{\partial E}{\partial \beta} + \frac{S}{\beta^2} - \frac{1}{\beta}\frac{\partial S}{\partial E}\frac{\partial E}{\partial \beta} - \frac{1}{\beta}\frac{\partial S}{\partial L_2}\frac{\partial L_2}{\partial \beta} - \frac{\gamma}{\beta^2}L_2 + \frac{\gamma}{\beta}\frac{\partial L_2}{\partial \beta}. \tag{40}$$

Using $\partial S/\partial E = \beta$ and $\partial S/\partial L_2 = \gamma$, we easily find

$$\frac{dF}{d\beta} = \frac{S}{\beta^2} - \frac{\gamma}{\beta^2}L_2, -\frac{d(\beta F)}{d\beta} = -\left(F + \beta\frac{dF}{d\beta}\right) = -E. \tag{41}$$

If we construct the stable branches for several values of $\gamma$, we can build up a general picture of the stability of the extremum solutions. We can apply the method for the case of a fixed $\beta$ as well. The extremum solutions are stable when $-\beta F$ is maximum:

$$\frac{dF}{d\gamma} = \frac{\partial E}{\partial \gamma} - \frac{1}{\beta}\frac{\partial S}{\partial E}\frac{\partial E}{\partial \gamma} - \frac{1}{\beta}\frac{\partial S}{\partial L_2}\frac{\partial L_2}{\partial \gamma} + \frac{1}{\beta}L_2 + \frac{\gamma}{\beta}\frac{\partial L_2}{\partial \gamma}, \tag{42}$$

$$\frac{dF}{d\gamma} = \frac{1}{\beta}L_2,$$

$$-\frac{d(\beta F)}{d\gamma} = -L_2. \tag{43}$$

From the results derived above we have a tool to separate the unstable solutions that is easy to apply. In the microcanonical ($E$-$L_2$) description, we have to inspect the extremum solutions in the $\beta$-$E$ plane for several fixed values of $L_2$ or in the $\gamma$-$L_2$ plane for several fixed values of $E$. However, in the $T$-$\gamma$ ensemble, we have to inspect the extremum solutions in the $(-E)$-$\beta$ plane for fixed $\gamma$ values, or we have to consider the extremum solutions in the $(-L_2)$-$\gamma$ plane for the case of fixed $\beta$. Either way, as we will show below, we can generalize the approach to two parameters.

## V. NUMERICAL METHOD

In order to find the entropy extremum solutions for the systems above, we have to solve Eq. (13) or (26), for the three-dimensional point mass system, or the three types of shell system. Generally, all of the differential equations can be written in the form

$$\frac{dy}{dr} = C\left(\frac{1}{r^2} + \Gamma\right)^{-n/2} e^{-\Psi(r)}, \tag{44}$$

$$\frac{d\Psi}{dr} = \frac{y}{r^2},$$

where $\Psi = \beta\Phi$ and $n = d - 1$ (as above, $d$ is the dimension of the system). Of course, the parameters $\Gamma > -1$ and $C > 0$ are different case by case. But it is quite interesting to mention that these systems behave similarly, regardless of whether we deal with a point mass system or a shell system, as long as the dimensions are the same. This is no longer a surprise if we look back at the Hamiltonians. But the similarity does also mean that, for example, a three-dimensional point mass system is equivalent to a three-dimensional shell system as far as the one-particle density function and the stability of solutions are concerned. Also, another advantage of the analogy is that we can dynamically model a three-dimensional point mass system with a three-dimensional shell system. Both systems should show the same equilibrium properties in the mean field limit. Of course, we have to reassign the moment of inertia of a shell to a different value in order to get *exactly* the same Hamiltonian in both cases.

The above system of equations should be solved with the following boundary conditions:

$$y(0) = 0, \tag{45}$$

$$\Psi(1) = -\beta.$$

Unfortunately, there are two things that make finding the solutions more difficult. First, Eq. (44) has a singularity at $r = 0$ and, secondly, the existence and uniqueness of the solution are questionable for any given $C$, $\beta$, and $\Gamma$. We cannot simply set $C$ and $\Gamma$ to satisfy our constraints of specified $E$ and $L_2$ because we do not have explicit forms of $E$ and $L_2$ in terms of $C$ and $\Gamma$: the constraints are functionals of $\rho$ and $\Phi$. To eliminate this problem we can change our boundary condition problem to an initial value problem because, in the latter case, we can ensure the existence and uniqueness of our solution for any $C > 0$ and $\Gamma > -1$. Therefore we choose

$$y(0) = 0, \tag{46}$$

$$\Psi(0) = \Psi_0,$$

where $\Psi_0 \in (-\infty, +\infty)$, and we are able to construct the solution around $r = 0$ in the form of a power series of $\Psi$ and $y$. From the numerical point of view, we should take the power series of $\Psi$ and $y$ in $r_1$ (a sufficiently small radius around $r = 0$), and then continue the integration of Eq. (44) numerically from that point with the new initial values

$$y(r_1) = y_{01}, \tag{47}$$

$$\Psi(r_1) = \Psi_{01}.$$

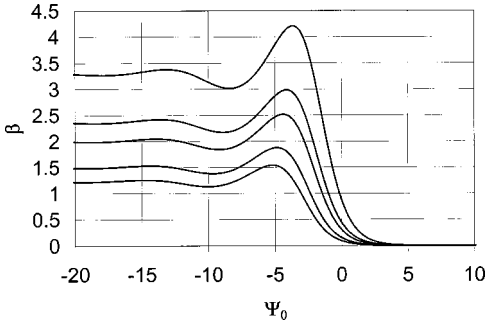


FIG. 1. The extremal solution curves at different values of $\Gamma = 2\gamma/\beta$ (from the top to the bottom $\Gamma = -0.9, -0.5, 0, 2, 5$.) Note that each curve has an upper bound $\beta_c(\Gamma)$, and no extrema can be found with $\beta > \beta_c(\Gamma)$. Also note that over a certain range of $\beta$ multiple solutions are present. However, of those multiple solutions, only those are stable that have the highest value of $\Psi_0$ (see Fig. 2 below). The asymptotic cases are $\Psi_0 \to -\infty$ [$\beta \to \beta_0$ and $\rho_V(r) \propto 1/r^2$] and $\Psi_0 \to \infty$, which is the high temperature limit.

Although the solution we get from Eq. (46) is unique, it does not satisfy both Eq. (45) and normalization. Looking at Eq. (44), we can see that we get all physical solutions with only one fixed $C = C_0$ for the initial value problem, since changing the value of $C$ is equivalent to shifting the solution, $\Psi$, by a constant. Therefore we can find all of the physically relevant solutions by fixing the value of $C$ and varying $\Psi_0$ and $\Gamma$. We also have to notice that, since we use $\Psi = \beta\Phi$, from the Poisson equation, the rhs of Eq. (44) is normalized to $\beta$, so we can get the inverse temperature by integrating Eq. (44), which is simply $y(1)$. In practice, we used the Bulirsch-Stoer method [22] to integrate the coupled, nonlinear, differential equations from $y_1$ and Bode's five-point method [22] to evaluate integrals. Relative errors were controlled to within $10^{-12}$.

## VI. NUMERICAL RESULTS

In Fig. 1 we show plots of $\beta$ vs $\Psi_0$ for the allowed extremal solutions corresponding to five particular values of $\Gamma$. The numerical results for the other models are qualitatively very similar, so we will use the point mass system to demonstrate their general features. As we can see, the solutions are bounded and, as a comparison, the results for the familiar isothermal sphere model ($\Gamma = 0$) [21,8] are presented as well. Examination of Fig. 1 clearly demonstrates the existence of an upper bound $\beta_c(\Gamma)$, which means that below a critical temperature there is no extremum solution at fixed $\Gamma$. In fact, this can be proved rigorously from the differential equations [23]. We can also see from the graph that $\dot{\beta}_c = d\beta_c/d\Gamma < 0$ and that, when $\beta \to \beta_0 = \lim_{\Psi_0 \to -\infty} \beta(\Psi_0)$, the number of solutions goes to infinity.

In Fig. 2 we show that three solutions occur for a particular value of $\beta$ ($=2.7$). At this point we do notknow which of them, if any, are stable. In Fig. 3 we plot the volume density profiles of these solutions normalized to the central density. As we can see, solutions represented by smaller $\Psi_0$ are more and more concentrated at the center. As a comparison, we also give the density profiles of the well known isothermal sphere ($\Gamma = 0$). There is some difference in the shape of the density profiles in the case where $\Gamma \neq 0$ but, in general, the volume density profile is singular as $\Psi_0 \to -\infty$, and has the asymptotic solution $\rho_V = 1/4\pi r^2$. Note that the linear density is $\rho = 1$ in this asymptotic case. In order to see the difference between density profiles of the isothermal sphere ($\Gamma = 0$) and

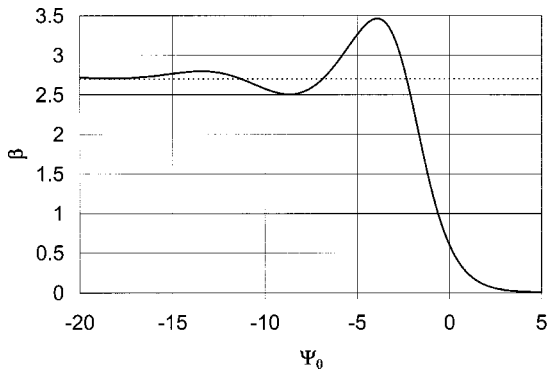


FIG. 2. The extremal solutions for $\Gamma = -0.74$. For $\beta = 2.7$, three extremum solutions are present, but only the one with the largest $\Psi_0$ is stable. For comparison, also see Fig. 8 below.

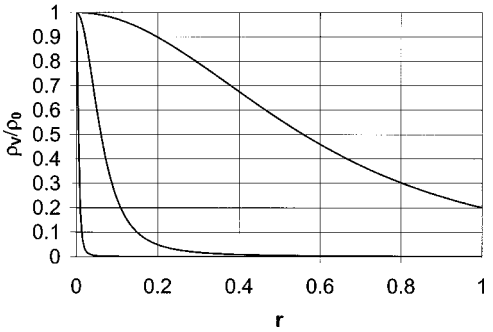


FIG. 3. The relative volume density profiles of the three extremal solutions in the case of the isothermal sphere ($\Gamma = 0, \beta = 2$). Only the least concentrated solution, which has the highest value of $\Psi_0$, is stable. The lower the value of $\Psi_0$, the more condensed and unstable the solutions become. The unstable solutions are characterized by a pronounced core-halo structure.

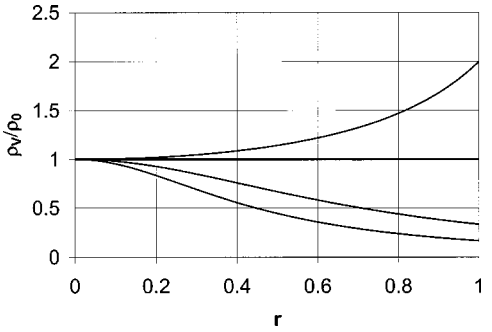


FIG. 4. In order to show the effect that a nonzero value of $\gamma$ has on the density, we plot the relative volume mass density profiles of the locally stable high temperature asymptotic solutions ($\Psi_0 \to \infty$) at different values of $\Gamma$ (from the top to the bottom, $\Gamma = -0.5, 0, 2, 5$). While the isothermal sphere has a constant density in this limit, nevertheless the models with $\Gamma \neq 0$ have different behavior due to the nonzero $\gamma$.

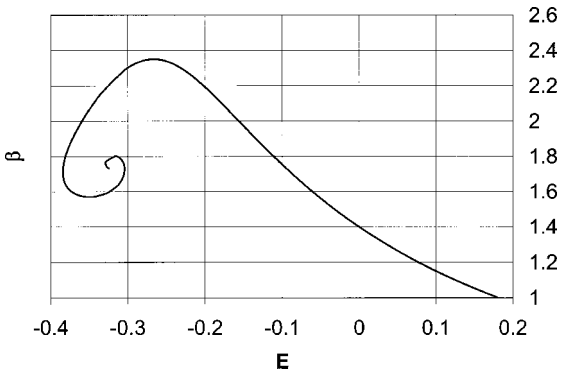


FIG. 5. The $\beta$ vs $E$ plot of the extremum solutions when $L_2=0.25$ ($E$-$L_2$ ensemble). As seen, there are no solutions below a critical value of the energy $E_c(L_2)$, and multiple solutions are present for a certain range of $E$. Based on the stability investigations, only the upper envelope of the complete spiraling curve $\Gamma \neq 0$ represents the stable solutions. Other pieces are unstable (more eigenvalues become negative) as we go to the center of the spiral. For comparison, see Fig. 7 below.

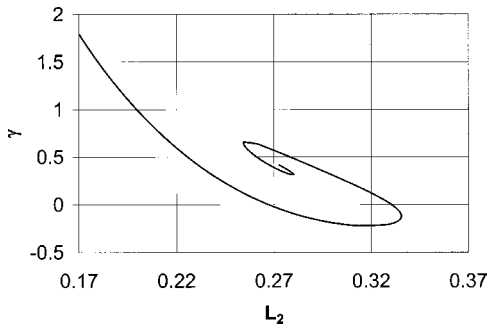


FIG. 6. The $\gamma$ vs $L_2$ plot of the extremum solutions when $E=-0.3$ ($E$-$L_2$ ensemble). Above a critical value of $L_2$, there are no extrema. In this case, the gravothermal catastrophe is also present according to the stability investigations, and only the first piece of the spiraling curve that starts at $L_2=0$ and ends at the critical value of $L_2$ defined above represents the stable solutions.

the others, we plot the high temperature solutions (Fig. 4). These are the $\Psi_0 \to \infty$ asymptotic solutions where $\beta \to 0$. If $\Gamma > 0$ the relative volume density profiles curve down, but when $\Gamma < 0$ the profiles curve up, indicating that, if we have an $l^2$ reservoir, at higher radius the density profile should change from the homogeneous density profile.

In order to show how the $L_2$ constraint affects the shape of the density profiles, in Fig. 4 we plot the relative volume density profiles for a high temperature. As we can see in the figure, when $\Gamma \neq 0$ the density profiles are no longer uniform and, depending on the sign of $\Gamma$, the density is either increasing ($\Gamma < 0$) or decreasing ($\Gamma > 0$), while in the standard case ($\Gamma = 0$) in the limit of high temperature the density is uniform. We can understand this behavior if we recognize that in the limit $\beta \to 0$ gravity can be neglected. Consider Eq. (10) when $\gamma \neq 0$. Since the kinetic energy contribution is still Maxwellian, the probability of finding a particle with large $l$ is smaller when $\Gamma > 0 (\gamma > 0)$, which means fewer particles will occupy larger radii. From the physical point of view, for a relatively large $L_2$, more particles should concentrate at larger radii in order to maintain the large value, while, for relatively small $L_2$, fewer particles should settle at large radii in order to balance the centrifugal forces. For the case where $\Gamma < 0$ the situation is the opposite, and the density profile should increase with increasing radius. Of course, while we cannot use this argument for finite temperatures, the origin of the difference in the density profiles when $\Gamma \neq 0$ is this effect. At finite temperature the tendency persists but the behavior is not guaranteed.

In Figs. 5 and 6, the stability properties are presented according to the previously discussed Poincaré linear series of equilibria with fixed $L_2$ and $E$ in the $E$-$L_2$ ensemble. As we can see, the gravothermal catastrophe holds for the $E$-$L_2$ ensemble as well. In Fig. 5, below a critical energy there is no extremal solution (here the radius is fixed, not the energy as in [4]). Also, at the same point, $\dot{\beta}_a(E_c) = \infty$ jumps to $\dot{\beta}_b(E_c) = -\infty$. (We follow the spiral in the counterclockwise direction.) Thus only the first branch, $a$, the upper envelope of Fig. 5, is stable. The other branches are increasingly unstable because additional eigenvalues become negative. In the opposite case, when we fix $E$ (Fig. 6), we can see that above a critical value of $L_2$ there is no extremum solution. The corresponding functions $S(E)$ and $S(L_2)$ are plotted in Fig. 7. We see that the entropy is monotonic above a critical energy in the stable region of the extremal solutions.

For the $T$-$\gamma$ ensemble, the results are presented in Figs. 8 and 9. First of all, in the case of fixed $\gamma$, we have to take a close look at the solutions in the $(-E)$-$\beta$ graph. Only the first branch of the solutions is locally stable up to a critical value of $\beta$, say $\beta_c$, because $(-\dot{E})_a(\beta_c) = \infty$, and there is no extremum for $\beta > \beta_c$. For given $\gamma < 0$, the existence condition now reads $\beta > 2|\gamma|$, inducing a positive lower bound on $\beta$. As a comparison, we selected the value of $\Gamma$ in Fig. 2 corresponding to Fig. 8; as we wind along the curve to a particular $\beta$ value, the extremum solutions are represented by a more concentrated set of density profiles. Another result of the stability investigations is that in Fig. 1, only those solutions are locally stable which are to the right of the largest maximum of the $\beta(\Psi_0)$ curves. The corresponding $-F$ can be seen in Fig. 10. In the stable region, it is a monotonic function, and therefore there is no sign of a phase transition. The same holds in the $E$-$L_2$ ensemble as can be seen by

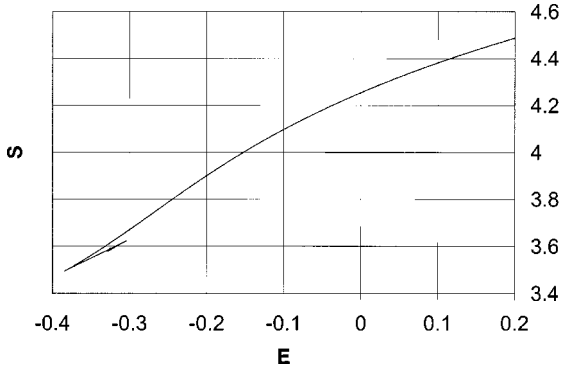


FIG. 7. The entropy vs energy curve for the case of $L_2=0.25$ ($E$-$L_2$ ensemble). (Also see Fig. 5.) The stable branch of the solutions in Fig. 5 can be identified as the highest entropy curve segment in the $S$ vs $E$ plot, which exactly ends at $E_c$. Note that this segment is also a monotonic function of $E$, which means no phase transition is present in the system.

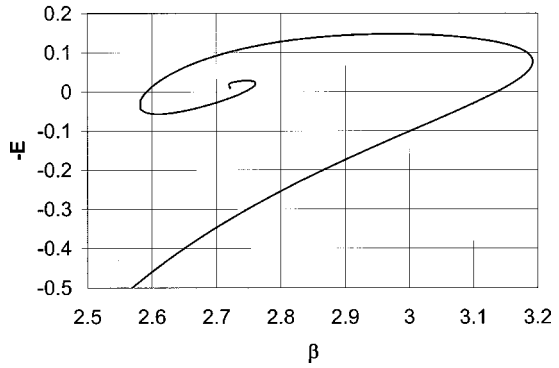


FIG. 8. The $(-E)$ vs $\beta$ plot of the extremum solutions in the $T$-$\gamma$ ensemble at $\gamma=-1$. There are no extrema above the critical $\beta_c(\gamma)$, and only the first branch of the extrema are stable. That piece of the spiraling curve which represents the stable solutions starts at $\beta=2$ and ends at $\beta_c$ (gravothermal catastrophe in the $T$-$\gamma$ ensemble). From Fig. 2, we can clearly see that only the least condensed density profiles represent the stable solutions. For comparison, see Fig. 10 below.

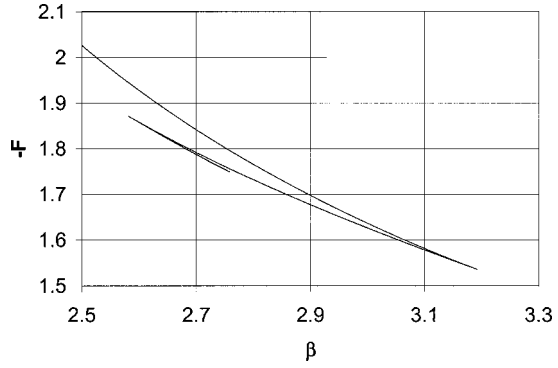


FIG. 10. $(-F)$ vs $\beta$ plot at fixed $\gamma=-1$, where $F$ is the thermodynamic potential in the $T$-$\gamma$ ensemble. From Fig. 8, we can clearly identify which piece of the curve represents the stable solutions; it is the first piece, starting at $\beta=2$ and ending at $\beta_c$. There is no sign of a phase transition because in the stable region $-F(\beta)$ is monotonic. Note that the stable solutions have the minimal $F$.

inspecting the entropy curves in Fig. 7. The results for fixed $\beta$ are shown in Fig. 9. The stable region of extremum solutions becomes unstable at $\gamma_c$ and at $\gamma>\gamma_c$ there are no extrema. The free energy behaves similarly to the case of fixed $\gamma$: it is monotonic and there is no phase transition.

## VII. CONCLUSION

The main purpose of this work is to study the equilibrium thermodynamics of spherically symmetric self-gravitating systems in the mean field limit. We investigated both the spherically symmetric point mass system and shell systems of differing dimension confined in a sphere. These systems are related to each other both in the form of their Hamiltonian and their equilibrium states. Furthermore, the *three*-dimensional shell system has the interesting and potentially useful property that, with regard to the equilibrium density profile, it is equivalent to the spherically symmetric point mass system. Our description is more general than the standard treatment of the isothermal sphere [21] since, in addition to the energy, we take into account $L_2$, the sum of the squares of the individual angular momenta, which is conserved in the mean field limit for spherically symmetric systems. In this type of microcanonical description ($E$-$L_2$ ensemble) we evaluated the ''equilibrium'' one-particle probability density function for each type of system by finding the extrema of the entropy. The resulting PDF's turned out to be similar to Eddington's anisotropic density function [16]. Therefore the density profiles obtained here also differ from those of the isothermal sphere which, in our formulation, is the special case $\gamma=0$. Near the system center, the density profiles are similar to those of the isothermal sphere. However, as the outer boundary is approached, depending on the value of $\Gamma$, deviations can become large, increasing or decreasing depending on the sign of $\Gamma$. The physics behind this behavior is simple: if the system is spun up corresponding to negative $\Gamma$, the outer density increases. If, on the other hand, the radial kinetic energy dominates the rotational energy, $\Gamma\cdot>0$ and the outer density decreases.

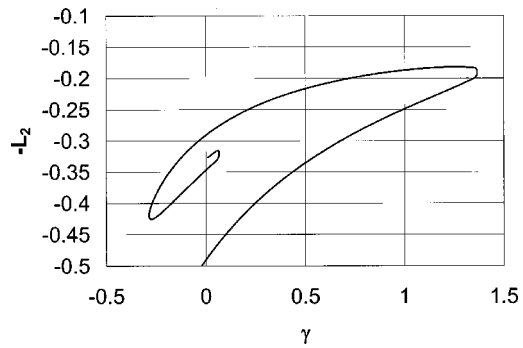


FIG. 9. The $(-L_2)$ vs $\gamma$ plot of the extremum solutions at $\beta=2$ ($T$-$\gamma$ ensemble). There are no extrema above the critical value $\gamma_c(\beta)$ and only the first branch of the extrema is stable. The curve segment that represents the stable solutions starts at $\gamma=-1$ and ends at $\gamma_c$. In other words, the gravothermal catastrophe is present.

In addition to the microcanonical ensemble, the Lagrange multiplier $\gamma$, which arose from the constraint on $L_2$, yielded a canonical ensemble ($T$-$\gamma$) that corresponds to the system being embedded in a heat bath at temperature $T$ and an $l^2$ reservoir at $\gamma$. But this analogy is correct only if the system is, at least, in a local equilibrium state, and this issue demonstrates the importance of checking the stability properties of the extremum solutions. The method known as Poincaré's linear series of equilibria proved adequate to analyze the stability of the extremum solution in both ensembles with a little extra effort. Using it, we showed that only certain types of solutions are locally stable, and others are saddle points. In other words, the gravothermal catastrophe is also present in both the $E$-$L_2$ and $T$-$\gamma$ ensembles, which means that there is no phase transition in our spherical mean-field models, although one was expected to be present because of the $L_2$ constraint.

From their description of the gravothermal catastrophe it is easy to imagine that Lynden-Bell and Wood [4] had in mind a dynamical process in which mass was transferred from the halo to a concentrated central core. However, their approach was confined to a comparison of stationary states. Hints of collapse have been seen in some *N*-particle simulations [24]. In future work we plan to study the complete dynamics of the collapse, both analytically and using dynamical simulation of *N*-particle and *N*-shell systems. The shell systems should prove especially useful since they avoid the complication arising from the formation of tight binaries [2].

## ACKNOWLEDGMENTS

The authors benefitted from conversations with Igor Prokhorenkov and Michael Kiessling. They also are grateful for the support of the Research Foundation and Department of Information Services of Texas Christian University.

[1] D. C. Heggie and G. Meylan, Astron. Astrophys. Rev. **8**, 1 (1997).
[2] J. Binney and S. Tremaine, *Galactic Dynamics* (Princeton University Press, Princeton, NJ, 1987).
[3] V. A. Antonov, Vestn. Leningr. Gos. Univ. **7**, 135 (1962).
[4] D. Lynden-Bell and R. Wood, Mon. Not. R. Astron. Soc. **138**, 495 (1968).
[5] J. Katz and D. Lynden-Bell, Mon. Not. R. Astron. Soc. **184**, 709 (1978).
[6] J. Katz, Mon. Not. R. Astron. Soc. **183**, 765 (1978).
[7] J. Katz, Mon. Not. R. Astron. Soc. **189**, 817 (1979).
[8] T. Padmanabhan, Astrophys. J., Suppl. Ser. **71**, 651 (1989).
[9] T. Padmanabhan, Phys. Rep. **188**, 285 (1990).
[10] F. Bavaud, Rev. Mod. Phys. **63**, 129 (1991).
[11] M. K.-H. Kiessling, J. Stat. Phys. **55**, 203 (1989).
[12] P. Hertel and W. Thirring, Ann. Phys. (N.Y.) **63**, 520 (1971).
[13] D. Lynden-Bell and R. M. Lynden-Bell, Mon. Not. R. Astron. Soc. **181**, 405 (1977).
[14] M. K.-H. Kiessling, B. Stahl, and K. Schindler, Planet. Space Sci. **43**, 271 (1995).
[15] B. N. Miller and P. Youngkins, Phys. Rev. Lett. **81**, 4794 (1998).
[16] A. S. Eddington, Mon. Not. R. Astron. Soc. **75**, 366 (1915).
[17] J. E. Gunn and R. F. Griffin, Astron. J. **84**, 752 (1979).
[18] M. Henon, Mem. Soc. R. Sci. Liege (V) **15**, 305 (1967).
[19] L. R. Yangurazova and G. S. Bisnovatyi-Kogan, Astrophys. Space Sci. **100**, 319 (1984).
[20] B. N. Miller and P. Youngkins, Phys. Rev. E **56**, R4963 (1997).
[21] S. Chandrasekhar, *An Introduction to the Theory of Stellar Structure* (Dover, New York, 1939).
[22] W. H. Press, S. A. Teukolsky, B. P. Flannery, and W. T. Wetterling, *Numerical Recipes in C* (Cambridge University Press, Cambridge, 1988).
[23] I. Prokhorenkov (private communication).
[24] A. A. El-Zant, Phys. Rev. E **58**, 4152 (1998).